CNRS
Centre National de la Recherche Scientifique

INFN
Instituto Nazionale di Fisica Nucleare

Mirror motion reconstruction for free swinging Michelson data

F.Marion, B. Mours, L. Rolland

VIR-112A-08

November 21, 2008

VIRGO * A joint CNRS-INFN Project
Project office: Traversa H di via Macerata - I-56021 S. Stefano a Macerata, Cascina (PI)
Secretariat: Telephone (39) 50 752 521 – Fax (39) 50 752 550 – e-mail virgo@pisa.infn.it

Contents

1 Introduction

The "free swinging Michelson" technique is the basis of the current Virgo actuator calibration. In this specific configuration, the mirror motion can be reconstructed. It is used to measure the actuation transfer function (m/V), i.e. the response of the suspended mirror to an excitation applied to its actuator. Some results of such analysis has been shown in [1], [2], [3] and [4].

In this note, the method used to reconstruct the mirror motion is described. The results of the reconstruction on simulated data are given as well as the sensitivity obtained on the Virgo data.

2 Mirror motion reconstruction

2.1 The free swinging Michelson configuration

The interferometer (IFO) is set in a simple Michelson configuration, with frontal phase modulation. In order not to have cavities, the PR mirror and one mirror per arm are misaligned as shown in the figure 1. Four configurations are possible:

- short Michelson: the IFO is set with the NI and WI mirrors.
- long Michelson: the IFO is set with the NE and WE mirrors.
- asymmetric Michelson: the IFO is set with the NE and WI or WE and NI mirrors.

In such a configuration, the phase difference $\Delta\Phi$ between the two recombined beams is related to the differential arm length ΔL, the laser wavelength λ being the reference length:

$$\Delta L = \frac{\lambda}{4\pi}\Delta\Phi \tag{1}$$

The mirrors used in the simple Michelson configuration are let free in the longitudinal direction (along the beam). They are thus freely swinging. In general, the mirror motion is enough (a few microns) to see the fringes going back and forth at the Michelson output. If they would be more stable, an excitation signal would have to be added.

2.2 Output signals

When the IFO is in a free swinging Michelson configuration, the output signals, i.e. the continuous (DC) and demodulated (ACp *in phase* and ACq *in quadrature*) powers, are functions of the phase difference $\Delta\Phi$ between the two recombined beams:

$$P_{DC} = \beta\big(1 - \gamma\cos(\Delta\Phi)\big) \tag{2}$$
$$P_{ACp} = \alpha_{ACp}\sin(\Delta\Phi) \tag{3}$$
$$P_{ACq} = \alpha_{ACq}\sin(\Delta\Phi) \tag{4}$$

where β, α_{ACp} and α_{ACq} are proportional to the laser power, and γ is proportional to the interferometer contrast. The calculations are given in the appendix B.

2.3 Mirror motion reconstruction

In the plane of a demodulated signal (ACp or ACq) versus the continous signal (DC), the measurements follow an ellipse as described by the equations 2 and 3 or 4. Examples of ellipse measured in the data are shown in the figure 2. The phase offset $\Delta\Phi$ between both arms is the

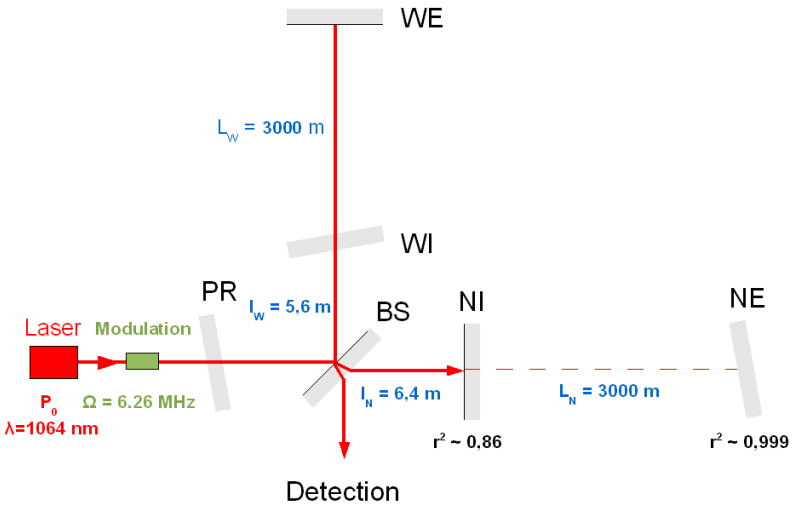

(a) Asymmetric Michelson WE-NI

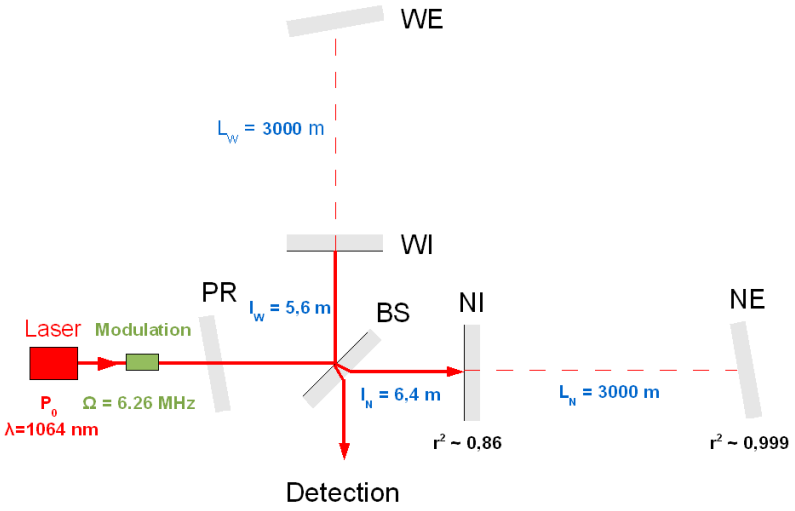

(b) Short Michelson NI-WI

Figure 1: Examples of Michelson configurations.

angle from the x-axis and the line from the ellipse center to the current data position along the ellipse. The differential arm length ΔL is then reconstructed from equation 1.

Two methods can be used to reconstruct the phase offset $\Delta\Phi$. One is based on the estimation of the minima and maxima of the different signals and is called hereafter the *MinMax* method. The other one is based on a fit of the ellipse parameters (center position and axis widths) and is called the *Ellipse* method.

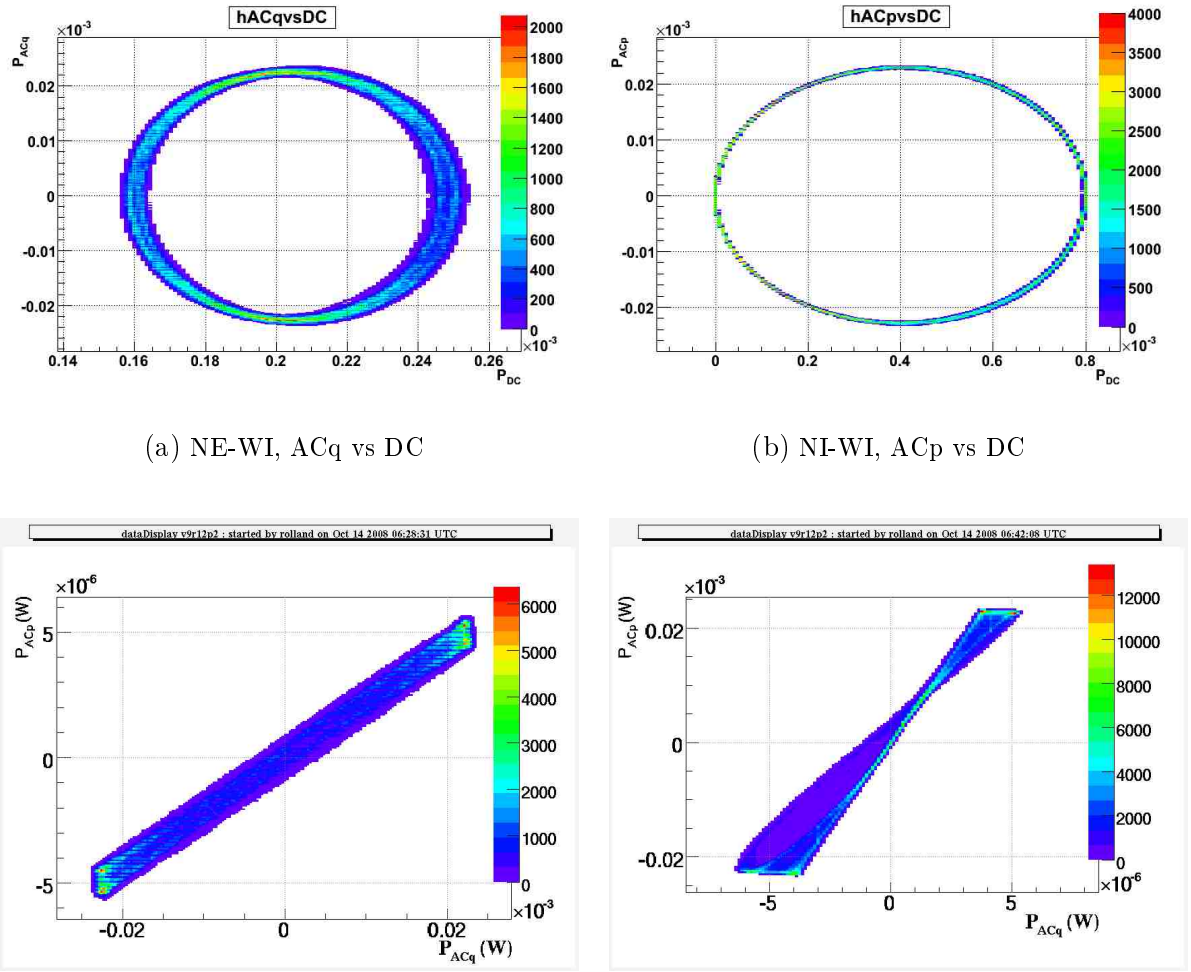

(a) NE-WI, ACq vs DC

(b) NI-WI, ACp vs DC

(c) NE-WI, ACp vs ACq

(d) NI-WI, ACp vs ACq

Figure 2: Examples of 2-dimensional plots of the continuous and demodulated photodiode signals. Data in NE-WI configuration: GPS 875586970, for 5 minutes. Data in NI-WI configuration: GPS 875588235, for 5 minutes.

2.3.1 MinMax method

This method is based on the estimation of the minima, maxima and average of the continuous and demodulated signals. Then, the α, β and γ parameters are computed:

$$\alpha = \frac{P_{AC}^{max} - P_{AC}^{min}}{2} \quad (5)$$

$$\beta = < P_{DC} > \quad (6)$$

$$\gamma = \frac{P_{DC}^{max} - P_{DC}^{min}}{2\beta} \quad (7)$$

$\Delta\Phi$ is then derived from:

$$\cos\Delta\Phi = \frac{\beta - P_{DC}}{\beta \times \gamma} \quad (8)$$

$$\sin\Delta\Phi = \frac{P_{AC}}{\alpha} \quad (9)$$

Details of the algorithm are described in appendix C.

The MinMax method has to be used on data with the full ellipse covered such that the minima, maxima and average values are well estimated. The current algorithm does not take into account the width of the ellipse due to the noise: the minima and maxima of the signal are thus absolute extrema. The parameters α and γ must thus be somehow overestimated.

The time series of the α, β and γ parameters are shown in the figure 3 for data in asymmetric NE-WI Michelson and in short Michelson configurations respectively. In order to compare with the raw signals, the data are the same as the one shown in the figure 2. The parameters are stable in the short Michelson data, and slightly varying in the asymmetric NE-WI data. However, the variations are lower than $\sim 5\%$. As shown in appendix B (table 5), the value of γ is expected to be close to the IFO contrast, 1 in the short Michelson configuration and 0.24 in asymmetric configurations. The measured values (~ 1 and ~ 0.22) are compatible with expectations within $\sim 10\%$. The expected value of β/P_0 are 0.22 and 0.44 (table 5). From the measured value of β, one can infer that the laser power impinging on the BS is of the order of 0.9 mW (is it expected so low ?).

2.3.2 Ellipse method

This methods is based on an ellipse fitting [5] of the two-dimension plot of the AC vs DC signals. The fit is regularly processed and gives the ellipse centre position (x_0, y_0) (theoretically $(\beta, 0)$) and the axis widths σ_x and σ_y normalized such that $\sigma_y = 1$ (theoretically $(-\beta\gamma/\alpha, 1)$). $\Delta\Phi$ can then be deduced directly[1]. The ellipse fitting process is working even if only a part of the ellipse (more than 1/4th yet) has been followed by the signal. The details of the algorithm are described in appendix D.

[1] Only the center position is necessary to compute $\Delta\Phi$

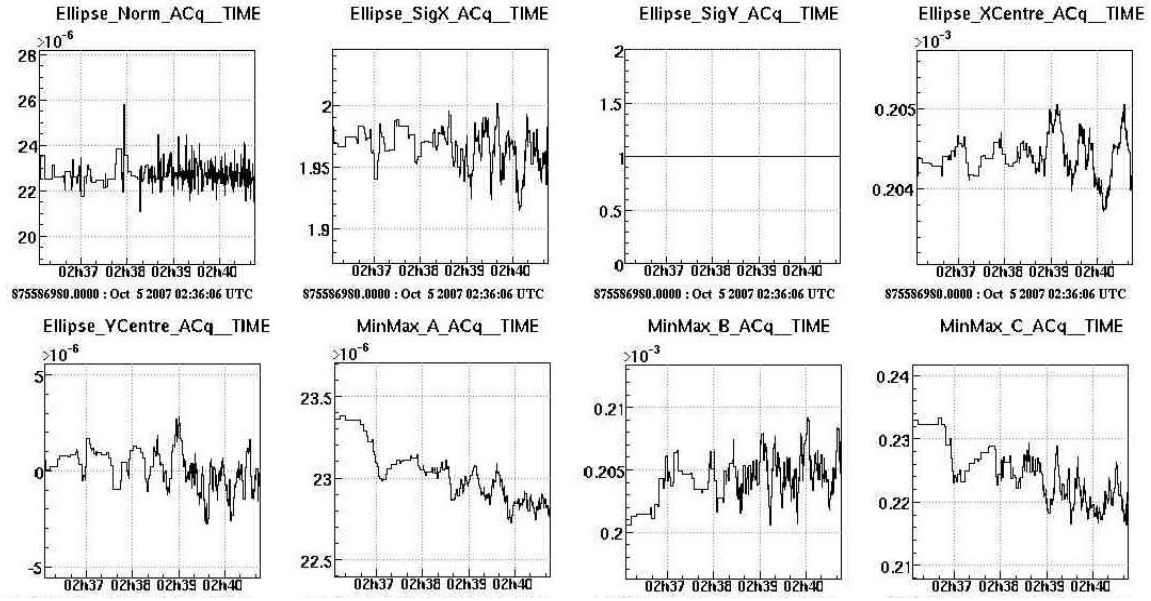

(a) Asymmetric NE-WI Michelson

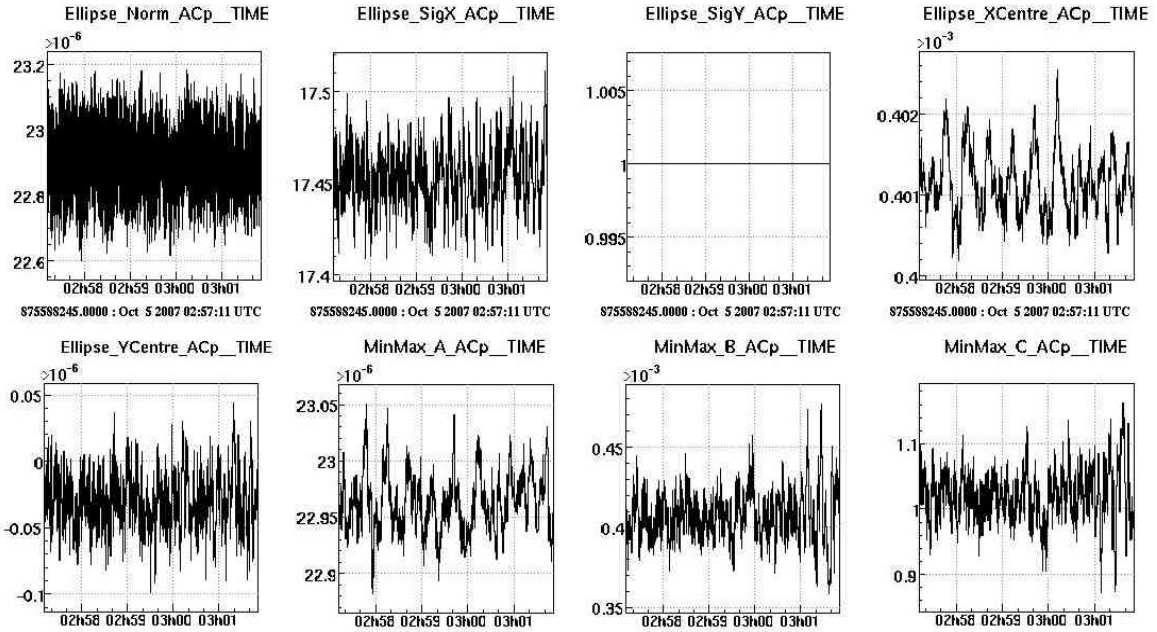

(b) Short NI-WI Michelson

Figure 3: Examples of time series of the parameters used in the reconstruction. The MinMax method channels for α, β and γ are called MinMax_A (W), MinMax_B (W) and MinMax_C. The Ellipse method channels are the ellipse center Ellipse_XCentre (W) and Ellipse_YCenter (W), the ellipse axis width Ellipse_SigX and Ellipse_SigY (set to 1 by the method) and the ellipse normalisation factor Ellipse_Norm.

The time series of the the estimated ellipse center position, axis width and ellipse size are shown in the figure 3 for data in asymmetric NE-WI Michelson and in short Michelson configurations respectively. The data are the same as the one shown in the figure 2. The values give a correct description of the ellipses. The important parameters for the estimation of $\Delta\Phi$ are the ellipse center position. A way to estimate their precision is to estimate the position variations over the ellipse width: $\frac{\Delta x_0}{\sigma_x \times N}$. In asymmetric Michelson configurations, where the ellipse contour is large (noisy), the precisions are of the order of 1% 10% along the DC and AC axis ; in short Michelson configuration, where the ellipse contour is much thinner, the precisions are of the order of 0.3% along both axis.

2.3.3 Rough check with fringe counting

The reconstructed ΔL can be checked comparing, on the same time window, the motion calculated from the algorithm and the motion estimated from the number of fringes passing in front of the photodiodes. The length offset from a fringe to the following one is expected to be $\frac{\lambda}{2}$. An example of reconstructed signal and DC photodiode signal is shown in the figure 4 (also in the figure 13 (p. 31)). Six intervals between bright fringes are passed within $\Delta t \sim 0.5$ s. It corresponds to a differential mirror motion of $\Delta L \sim 6\frac{\lambda}{2} = 3.19\,\mu$m. At the same time, the reconstructed signal shows a differential motion of $\Delta L \sim 3.18\,\mu$m as expected. This check validates the reconstruction process.

2.3.4 Some remarks

Since the sign of α in equations 3 and 4 is not known (the phase difference between the signal and the demodulation phase is not measured), the absolute sign of $\Delta\Phi$ and therefore ΔL cannot be determined by this method.

In principle, the demodulation phase Ψ (see equations 34) could be set such that one of the demodulated power is null while all the information is contained in the other one. This could increase the sensitivity of the free swinging Michelson data. Another way to extract all the information from both demodulated signals is to use a combination of both (i.e. $P_{AC} = sign(P_{AC_p})\sqrt{P_{AC_p}^2 + P_{AC_q}^2} \propto \sin(\Delta\Phi)$). It has been tested but the reconstructed ΔL was slightly noisier than using one of the demodulated signal alone.

The larger noise in asymmetric configurations compared to the short configuration (see the width of the ellipse contours) must be due to alignement noise. When a 3-km arm is used, the alignement variations of the end mirror must change the beam matching on the BS. This has to be checked looking at the alignement signals in the future data for Virgo+ calibration since these signals were not saved in the Virgo calibration data stream.

When a dominant excitation is injected to an arm mirror actuation, the reconstructed ΔL

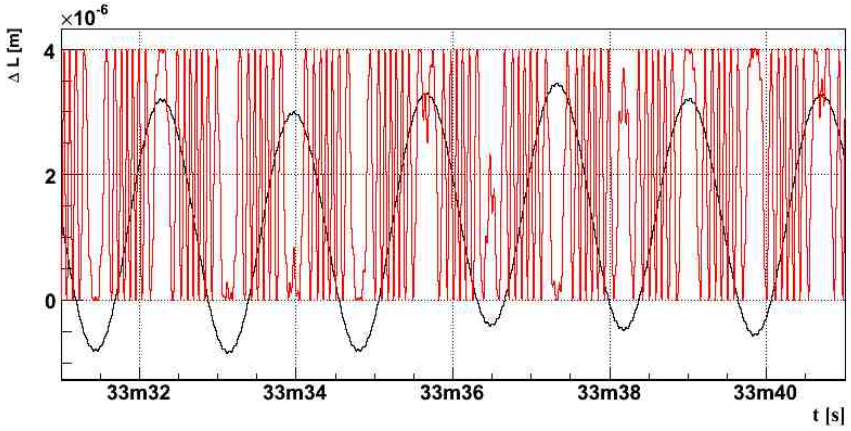

(a) 10 s of NI-WI data

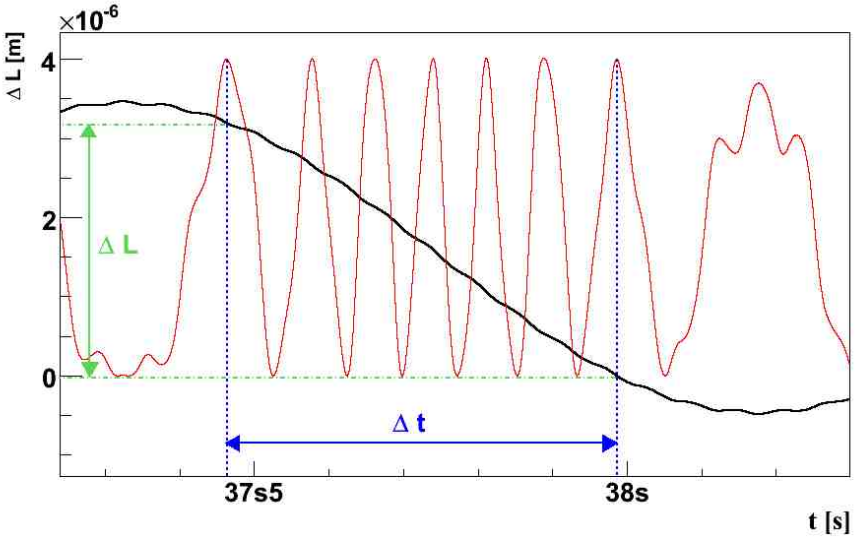

(b) Counting the fringes over 1 s

Figure 4: Comparison of the reconstructed signal ΔL (black) with the scaled DC signal measured on the B1p photodiode (red, its range goes from 0 to 0.8 mW). Six interfringes are seen during the time Δt. They correspond to a differential displacement ΔL.

at the correspondant frequencies gives the motion of this mirror. When injected to the BS mirror, an effective motion is reconstructed. Since the mirror is inclined by 45°, a real longitudinal mirror displacement of Δl_{BS} increases one arm length by $\Delta l \cos(45°) = \Delta l\sqrt{2}/2$ while decreasing the other arm length by the same amount. The effective differential arm length that is reconstructed is thus $\Delta L_{BS} = \sqrt{2}\Delta l_{BS}$.

The reconstruction method is not expected to induce any delay between the $\Delta L(t)$ signal and the photodiode signals. However, a delay is expected from the mirror motion to the photodiode signals due to the light propagation time is the arms. This delay is negligible from the central mirrors (NI and WI) but must be $10\,\mu$s from the WE and NE mirrors. For the BS mirror, the case is more difficult: the beam transmitted by the BS to the north arm is reflected on the north mirror and 'sees' the BS position when it is reflected to the photodiodes ; the beam reflected by the BS to the west arm 'sees' the BS position when it enters the interferometer, and is then propagated back and forth in the west cavity, and transmitted by the BS mirror to the photodiodes. No delay is expected from the first beam, while a delay of $20\,\mu$s is expected from the second beam when the long arm (up to WE) is used. The effect on the phase when both beams are recombined cannot be easily calculated. It has been estimated using simulations later in this note.

3 Checks and performance of the reconstruction

Additionnal checks and performance estimation of the ΔL reconstruction are evaluated in this section.

From the motions of the mirrors to the output photodiode channels used for the ΔL reconstruction, the signal processes through the optical response of the IFO, which depends on the mirrors, and through the photodiode readout electronics. The effect of the IFO optical response and the effect of possible non-flat response of the photodiode readout electronics are estimated.

The sensitivity of the free swinging Michelson data is then estimated.

3.1 Effect of the IFO optical response

The optical response is expected to be a delay due to the light propagation time from the mirror to the detection photodiodes. A special case arises for the motion of the BS motion in configurations using the WE mirror. In this case, the BS mirror motion is probed by the IFO laser beam twice as shown in the figure 5: when the input beam is reflected towards the WE mirror, this beam travels $20, \mu$s before it is recombined on the BS ; when the beam coming back from the north arm is reflected on the BS towards and recombined with the west arm beam to the detection. The simulations are used to check the expected optical response and to determine the response in the particular case of the BS.

Simulated data of free swinging Michelson configurations have been computed with the SIESTA code [6] using the OPseq simulation[2] for the interferometer with a clock at 1 MHz (see appendix F for a configuration file). The light propagation time in the central IFO are neglected ($\sim 30\ ns$, for distances of the order of 10 m). An excitation signal[3] is applied to one mirror actuation. The mirror motion is stored into the channel ΔL^{mir}_{simu}. The output of the detection photodiodes are also stored. The ΔL reconstruction algorithm is processed on these data, producing a channel ΔL_{rec}.

The TF $\frac{\Delta L_{rec}}{\Delta L^{mir}_{simu}}$ is computed in order to check the expected modulus and delay. The coherence of both signals is high from a few Hz to 10 kHz. Some examples are shown in the figure 6. Fits of a constant value and of a line has been done on the modulus and the phase respectively to extract the gains and delays.

For the arm mirrors, the modulus are flat and compatible with 1 up to 10 kHz. The delays are 0 for the input mirrors and $10\,\mu$s for the end mirrors as expected from the light propagation time. For the BS mirror, when the WI mirror is used in the Michelson configuration, the modulus is flat and compatible with $\sqrt{2}(\sim 1.414)$ up to 10 kHz and the delay is 0 as expected.

When the WE mirror is used, the simulations shown that the modulus of the TF of the BS mirror motion is not flat as shown in the figure 6(c). A fit of a complex pole (second order low-pass filter) has been computed on figure 7. The results are a gain of 1.414, a delay of

[2] with the option *full* set to YES

[3] white noise or white noise filtered by a pole and a zero

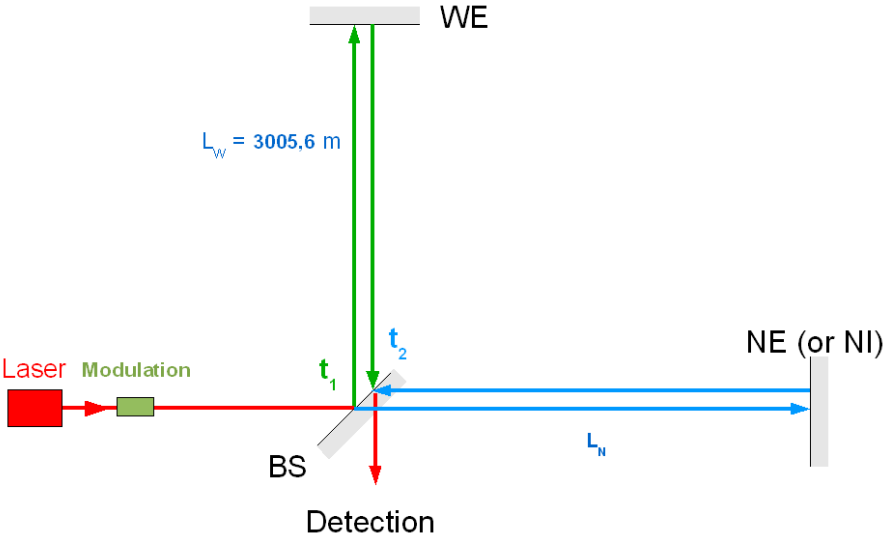

Figure 5: In NI-WE or NE-WE configurations, the position of the BS mirror is sensed at two different times. It is sensed when the input beam is reflected towards the WE mirror (green path), at t_1. After propagation in the arm, the beam is recombined with the beam coming from the north arm (blue path) at $t_2 \sim t_1 + 2 \times 10\,\mu$s. The beam coming from the north arm sense the BS mirror position when it is reflected on the mirror and recombined with beam from the west arm, at t_2. The recombined beam is then received by the detection photodiodes.

$-7.48\,\mu$s, a pole at 15460 Hz with a quality factor of 0.59. The residuals of the fit are better than 0.5% up to 5 kHz. However, the phase can be described by a delay of $10\,\mu$s up to 10 kHz within 10 mrad. The modulus can be assumed to be $\sqrt{2}$ within 0.2% up to 1 kHz.

The gains and delays of the different TFs between the reconstructed mirror motion and the effective one are summarized in the table 3. The delays correspond to the optical response of the IFO: it is the light propagation time in the arms. The simulations confirm that the reconstruction method does not introduce any systematic frequency dependence in the TF modulus nor in the phase below 10 kHz, excepted for the BS mirror in NE-WE and NI-WE configurations where frequency dependence is seen above 1 kHz.

Config.		BS	NI	WI	NE	WE
NI-WI	G	1.414 ± 0.018	0.996 ± 0.033	0.999 ± 0.039	-	-
	t_d	0.0001 ± 0.01	0	0	-	-
NE-WI	G	1.414 ± 0.018	-	1.000 ± 0.015	1.000 ± 0.014	-
	t_d	0	-	0	10.02 ± 0.27	-
NI-WE	G	$1.409 \pm 0.034(*)$	1.000 ± 0.013	-	-	1.000 ± 0.012
	t_d	$10.00 \pm 0.27(+)$	0	-	-	10.01 ± 0.23
NE-WE	G	$1.414 \pm 0.060(*)$	-	-	$\pm$	$\pm$
	t_d	$10.0 \pm 1.5(+)$	-	-	$\pm$	$\pm$

Table 1: Gains G and delays t_d in μs found between the reconstructed ΔL and the simulated mirror motion for the different simple Michelson configurations. They are valid up to 10 kHz, except for the gain of the BS mirror in NI-WE and NE-WE configurations, where they are valid up to $\sim$ 1 kHz. (*) Fit flat modulus below 1 kHz. (+) From a linear fit of the phase up to 10 kHz.

3.2 Effect of the readout electronics

A possible source of systematic errors is a bad compensation of the compression filters in the photodiode readout electronics. Simulations have been computed processing the photodiode output signals through some filters to distort the signal before using it in the ΔL reconstruction process. The 'bad compensation' has been simulated by a pole and a zero at 145 Hz and 150 Hz respectively[4]

When only the DC signal is filtered, the reconstructed ΔL loose coherence with the simulated mirror motion from $\sim$ 100 Hz to $\sim$ 2 kHz as shown in the figure 8. Around this region, the motion is properly reconstructed.

When only the AC signal is filtered, the effect is similar.

[4] Pole at 145 Hz: USfilter1 d1tmp d1.dc 0 0 911.1 1. 911.1
Zero at 150 Hz: USfilter1 d1new d1tmp.out 0 1 942.5 0. 942.5

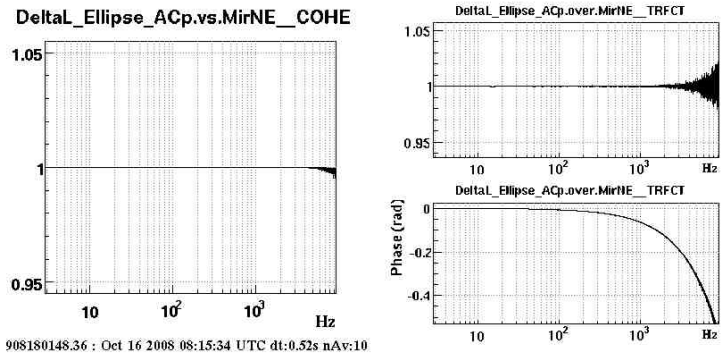

(a) NE-WI, injection on NE

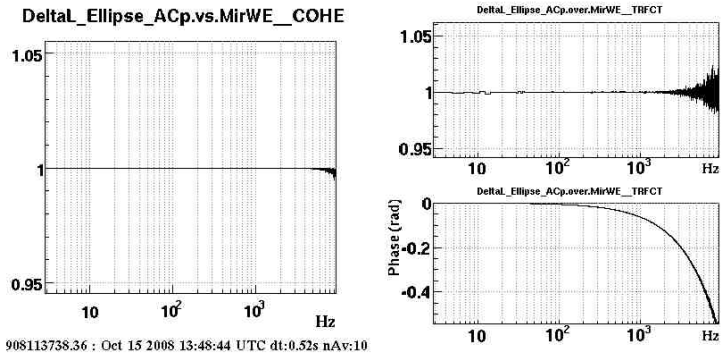

(b) WE-NI, injection on WE

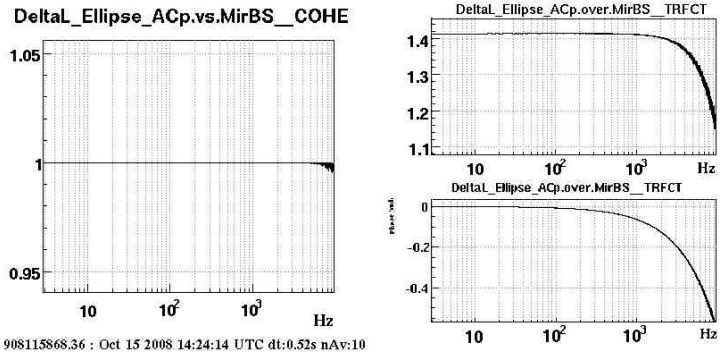

(c) WE-NI, injection on BS

Figure 6: Coherence and TF of the reconstructed from the simulated mirror motion to the reconstructed ΔL.

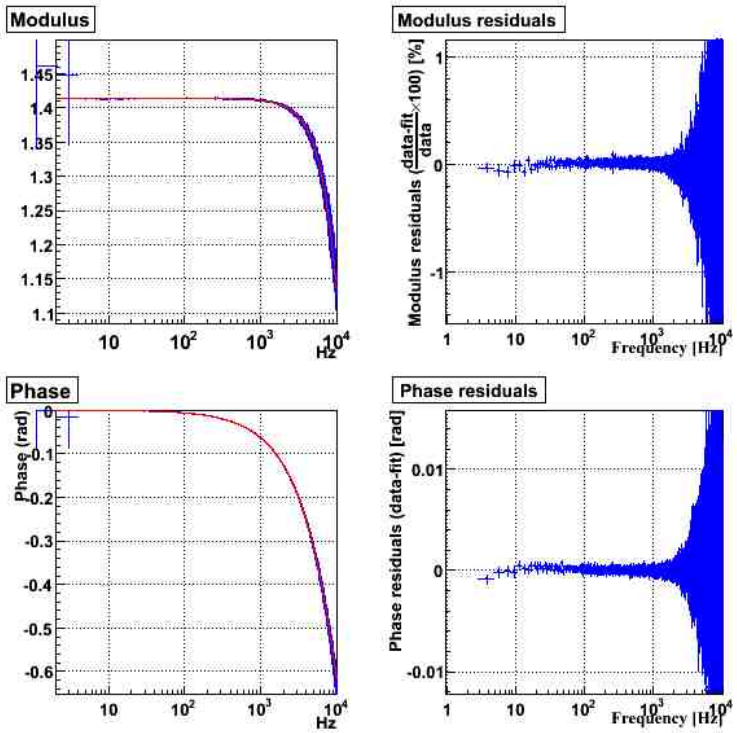

Figure 7: Fit of the TF of the reconstructed from the simulated BS motion to the reconstructed ΔL in NI-WE (and NE-WE) Michelson configuration. The residuals are also given.

When both the DC and AC signals are filtered with the same filters, the coherence between the reconstructed and simulated ΔL is close to 1 and the motion is properly reconstructed in all the frequency range.

These simulations have shown that it is important to have a precise compensation of the compression/decompression filters in the photodiode readout electronics in order not to loose sensitivity.

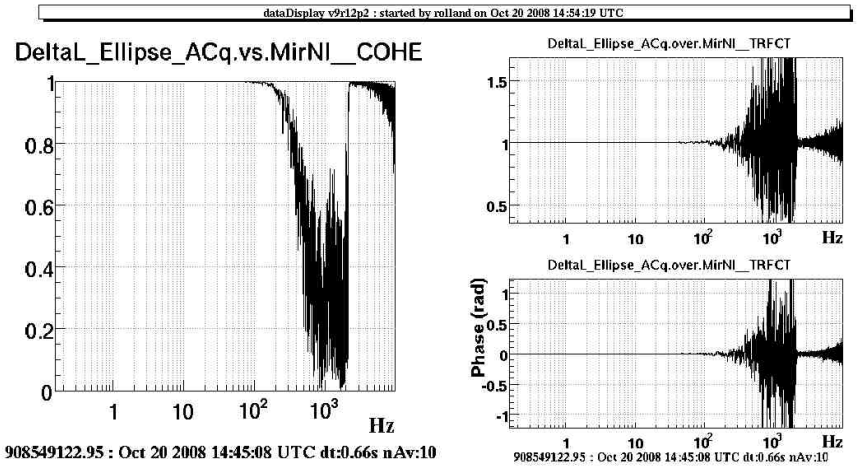

Figure 8: Coherence and TF of the reconstructed from the simulated NI mirror motion ΔL in NI-WI configuration, with a filter (pole and zero) applied to the readout DC photodiode signal.

3.3 Sensitivity to mirror motion

The sensitivity of the free swinging Michelson data is estimated. First, some tests are performed on simulated data. Then, examples of sensitivity obtained on real data are given.

3.3.1 Noise from the reconstruction

Free swinging short Michelson data without noise has been simulated, injecting a white noise to the NI mirror actuation. The WI and BS mirrors are fixed. In the simulations the demodulated signals are related by $P_{ACq} = -P_{ACp}$. The mirror motion level is described by the FFT of the simulated NI mirror as shown in the figure 9. The FFTs of the reconstructed signals have been superposed for comparison. Decreasing levels of white noise have been injected down to when the level of the reconstructed ΔL do not decrease any more. This lower level is assumed to described the noise floor from the reconstruction procedure.

Noise levels are similar for both *MinMax* and *Ellipse* methods, with a value of $10^{-12}\,\mathrm{m}/\sqrt{\mathrm{Hz}}$ at 150 Hz.

3.3.2 Sensitivity in real data

The sensitivity of the reconstructed free swinging Michelson data is estimated by the FFT of the reconstructed ΔL channel. It is shown in the figure 10. The best sensitivity of 10^{-12} m is achieved above 200 Hz. The lines below 1 kHz are calibration lines as quoted in the figure caption. A broad structure is visible between 4260 and 4320 Hz in all the data. Its origin is unknown (aliasing of the laser modulation frequency, or of a mirror drum mode ?).

The sensitivity is slightly better using the *Ellipse* method than the *MinMax* method. Also, depending on the Michelson configuration, one of the demodulated signal has a better sensitivity: ACq for asymmetric configurations and ACp for short Michelson configuration.

The origin of the noise is not understood yet. Possible origins are shot noise, laser frequency noise or alignement noise. The corresponding channels were not stored in the past calibration data. This study will be performed on the forthcoming Virgo+ free swinging Michelson data.

3.4 Search for non-linearities

A possible source of error could arise if the reconstruction method would introduce non linearities. This would show up as harmonic lines in the FFT of the reconstructed ΔL channel. Such lines were not found in the data. The table 2 gives the amplitude of a few lines and the noise level at its first multiple frequencies. It shows that possible non-linearities are below 0.1% of the initial line amplitude.

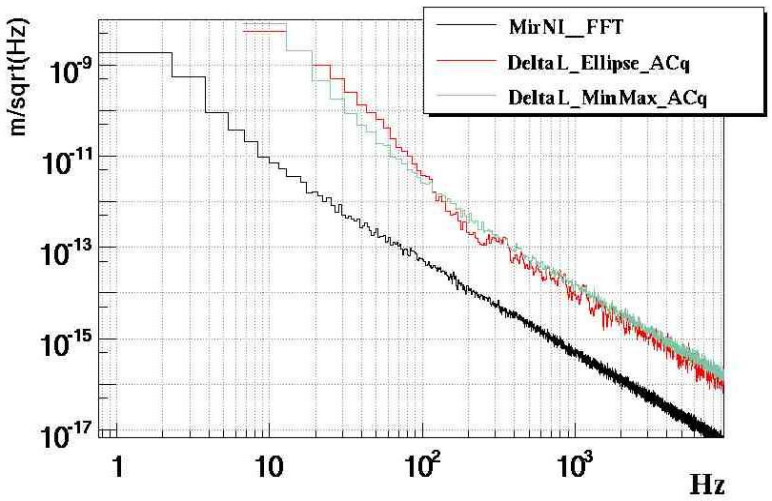

Figure 9: Lower achieved level of the FFT of the reconstructed ΔL signal (in $\frac{m}{\sqrt{Hz}}$) using both MinMax and Ellipse method, superposed onto the FFT of a low-amplitude simulated NI mirror motion.

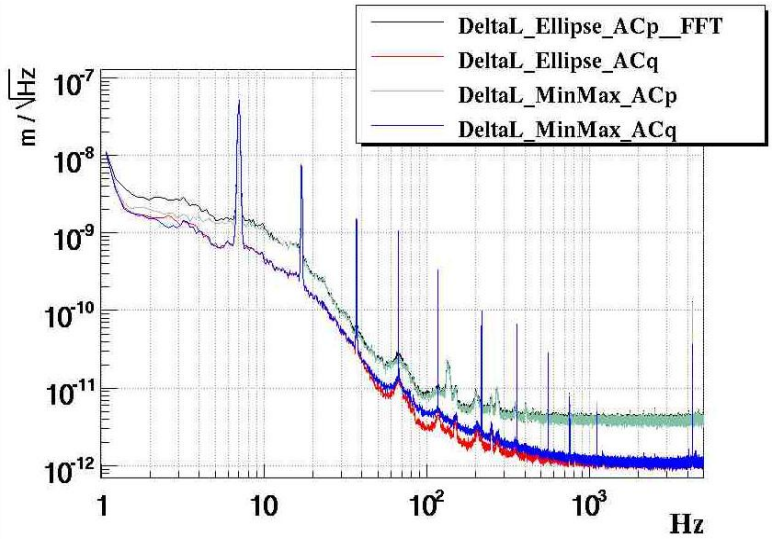

(a) Asymmetric NE-WI Michelson

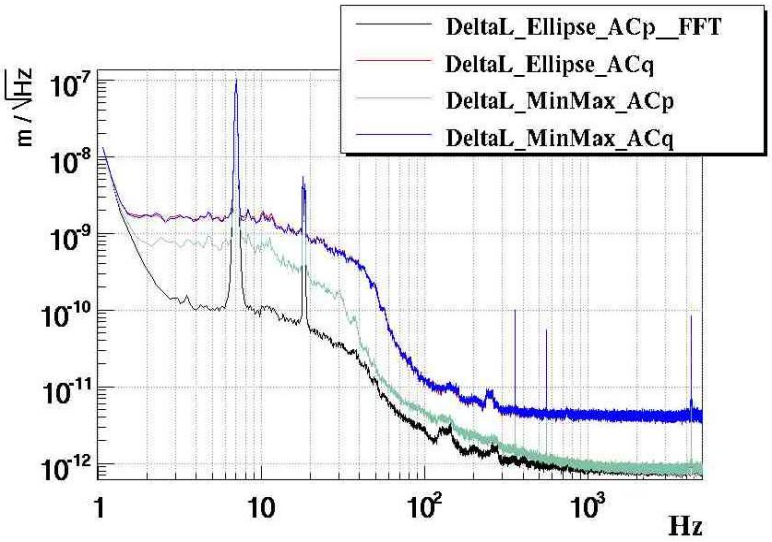

(b) Short NI-WI Michelson

Figure 10: FFT of the reconstructed ΔL signal (in $\frac{m}{\sqrt{Hz}}$) using both MinMax and Ellipse method, and both ACp and ACq signals (reconstruction sensitivity). Top: asymmetric NE-WI configuration (calibration lines were injected at 6.5, 16.5, 36.5, 66.5, 116.5, 8, 7, 17, 37, 67, 117 and 217 Hz). Bottom: short WI-NI configuration (calibration lines were injected at 7, 357, 557, 18 and 18.5 Hz).

	f_0 (Hz)	$A(f_0)$ (m/$\sqrt{\text{Hz}}$)	$A(2f_0)$ (m/$\sqrt{\text{Hz}}$)	$A(3f_0)$ (m/$\sqrt{\text{Hz}}$)	$A(4f_0)$ (m/$\sqrt{\text{Hz}}$)
NE-WI	7	5×10^{-8}	3×10^{-10}	1.4×10^{-10}	6.3×10^{-11}
NE-WI	67	1×10^{-9}	3.2×10^{-12}	3.1×10^{-12}	-
NE-WI	756	8.5×10^{-12}	1×10^{-12}	1×10^{-12}	-
NI-WI	7	9.6×10^{-8}	6.7×10^{-11}	5.4×10^{-11}	3.3×10^{-11}

Table 2: Amplitude of the injected line (f_0) and noise level at the first possible harmonics of the line.

4 Sensitivity to calibration signals

The noise level of asymmetric data as well as the maximum amplitude of calibration lines that can be injected for Virgo and Virgo+ (after the magnets and coil driver replacements) are compared in the figure 11. The reduction of actuation dynamic for Virgo+ might make impossible direct measurements of the actuation above 1 kHz.

The lines injected on the BS mirror can be stronger than for the arm mirrors, as seen on the figure.

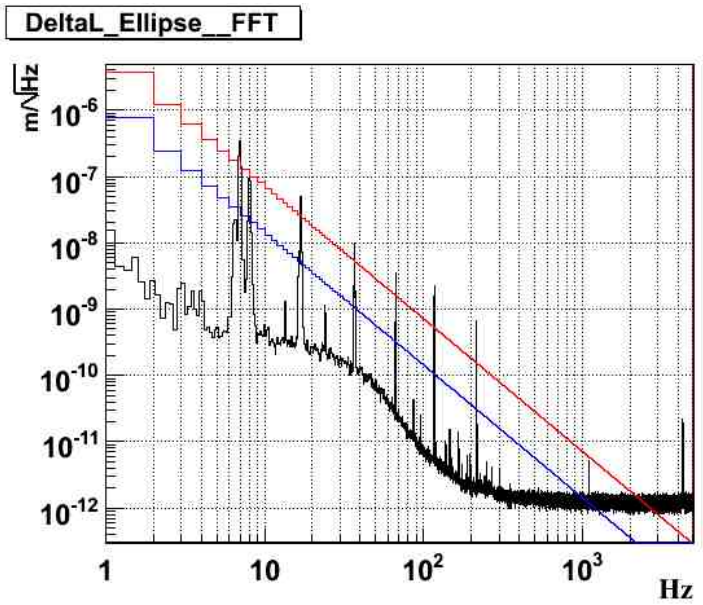

Figure 11: FFT of the reconstructed ΔL signal from WE-NI asymmetric Michelson data (100 s). The red curve indicates the maximum amplitude of calibration lines that can be injected to the end mirrors of Virgo, averaging 10 s-FFTs. The blue curve represent the amplitude for Virgo+ actuation, which is reduced by a factor ~ 5.

4.1 Possible improvements

Improvements in the sensitivity of the free swinging Michelson data might be possible:

- adjust the demodulation phase of the B1p photodiodes such that one demodulated signal is null, while all the information for the reconstruction is contained in the other one.
- increase the laser power. This would increase the size of the ellipses, improving the relative precision on the ellipse parameters or minimum/maximum values.

If the ellipse width is found to be due to alignement noise, possible alignement improvements for Virgo+ might also improve the sensitivity.

5 Conclusion

Two methods to reconstruct the differential mirror motion of a free swinging Michelson interferometer with frontal phase modulation have been described. They use the DC and a demodulated signal transmitted by the IFO.

Simulations were performed to check the reconstruction process. Both methods reconstruct the mirror motion without systematic effects nor time delay introduction. The optical response of the IFO has been characterised from the simulations.

The noise level obtained in the data has still to be explained. It will be studied on future free swinging Michelson data since not all the needed channels were stored in the past data. When the noise origin will be understood, a further version of this note will be done.

The sensitivity of the data to calibration signals has been studied. It has shown that the calibration-induced mirror motion might not be detectable above 1 kHz for Virgo+.

A Some Virgo mirror and cavity characteristics

During VSR1, the laser was phase-modulated at $\Omega = 6.264288\,\mathrm{MHz}$ with a modulation depth m varying[5] between 0.27 and 0.29.

The following tables give some intensity reflectivity and transmission coefficients values and the lengths of the different cavities.

PR	$R = 1.8 \pm 0.2\,\mathrm{ppm}$ (1st face) $T = 5.13\% \pm 0.02\%$ (2nd face)
BS	$R = 50.25\% \pm 0.18\%$ (1st face) $R = 519 \pm 10\,\mathrm{ppm}$ (2nd face)
NI	$R = 132 \pm 2\,\mathrm{ppm}$ (1st face) $T = 11.8\% \pm 0.03\%$ (2nd face)
NE	$T = 42.9 \pm 0.2\,\mathrm{ppm}$
WI	$R = 171 \pm 0.6\,\mathrm{ppm}$ (1st face) $T = 11.66\% \pm 0.02\%$ (2nd face)
WE	$T = 38.3 \pm 0.7\,\mathrm{ppm}$

Table 3: Intensity reflection and transmission coefficients of the Virgo mirrors.

l_{rec} (PR to BS)	5.98
l_n (BS to NI)	6.512
l_w (BS to WI)	5.634
L_N (NI to NE)	3000.0812
L_W (WI to WE)	3000.0812

Table 4: Lengths of the Virgo cavities, in meters. L_N and L_W are averaged on the west and noth cavities.

[5] During VSR1, the modulation depth was monitored in the channel $Bs\_MOD\_E0\_M6$, where the value 6.5 corresponds to $m = 2.7$ as measured in February 4th 2008 by Julien Marque.

B Calculation of continuous and demodulated powers for a Michelson interferometer

The aim of this annexe is to calculate the continuous and demodulated powers transmitted by a simple Michelson interferometer with frontal phase modulation. The results are used to reconstruct the mirror differential motion of the interferometer in the Virgo calibration.

First, the results for a simple interferometer without modulation are given. The frontal phase modulation is then added.

B.1 Michelson interferometer

In a Michelson interferometer, a beam is split into two arms by a beam splitter (BS) as shown in the figure 12 (no modulation is assumed yet). At the end of each arm, a mirror reflects the beams to the BS where they interfere.

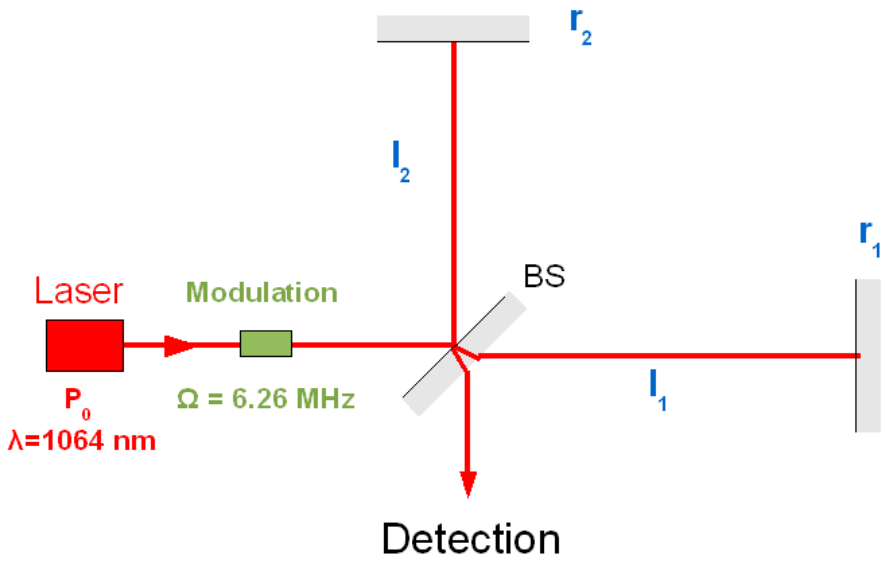

Figure 12: Simple Michelson configuration with frontal phase modulation

Let's call A the amplitude of the incident field on the BS (assumed ideal: $r = t = \frac{1}{\sqrt{2}}$). The

amplitude A^t of the beam transmitted to the detection is thus[6]:

$$\begin{aligned} A_t &= A(\frac{1}{\sqrt{2}})e^{jkl_1}(-r_1)e^{jkl_1}(\frac{1}{\sqrt{2}}) + A(\frac{-1}{\sqrt{2}})e^{jkl_2}(-r_2)e^{jkl_2}(\frac{1}{\sqrt{2}}) \\ &= -\frac{A}{2}\big[r_1 e^{2jkl_1} - r_2 e^{2jkl_2}\big] \end{aligned} \tag{10}$$

where $k = \frac{2\pi}{\lambda}$, λ the laser wavelength, l_1 and l_2 the arm lengths and r_1 and r_2 the amplitude reflection coefficients of the mirrors. In practice, the coefficients are effective coefficients that take into account the possible transmission coefficients when crossing the input mirrors and the beam matching which might not be perfect in a free swinging Michelson. With $l_- = l_2 - l_1$ the length difference and $l_+ = l_2 + l_1$ the sum of the arm lenghts, the amplitude of the transmitted field can be written:

$$A_t = Ae^{jkl_+}\big[jr\sin(kl_-) + \Delta r\cos(kl_-)\big] \tag{11}$$

where $r = \frac{r_1+r_2}{2}$ is the average reflectivity and $\Delta r = \frac{r_2-r_1}{2}$ the asymmetry between the two arm reflectivities.

The power transmitted by the interferometer is then:

$$\begin{aligned} P_t &= A_t\overline{A_t} \\ &= A\overline{A}\big[\Delta r^2\cos^2(kl_-) + r^2\sin^2(kl_-)\big] \\ &= A\overline{A}\big[\Delta r^2\frac{1+\cos(2kl_-)}{2} + r^2\frac{1-\cos(2kl_-)}{2}\big] \\ &= \frac{P_{max}}{2}\big[1 - C\cos(2kl_-)\big] \end{aligned} \tag{12}$$

with

$$P_{max} = P_0(r^2 + \Delta r^2) \qquad (\text{where } P_0 = A\overline{A}) \tag{13}$$

$$C = \frac{r^2 - \Delta r^2}{r^2 + \Delta r^2} \tag{14}$$

C is the interferometer contrast. The transmitted power is maximum $P_t = P_{max}$ when $2kl_- = (2q+1)\pi$ where q is an integer. The transmitted power is minimum $P_t = P_{min}$ when $2kl_- = 2q\pi$. We have: $\frac{P_{min}}{P_{max}} = \frac{1-C}{1+C}$.

B.2 Michelson with frontal phase modulation

A Pockels cell is set in front of the interferometer in order to modulate the phase of the laser beam before it enters the interferometer as shown in the figure 12. The phase is modulated

[6] The reflection coefficient r on a surface depends of the refraction indexes n_1 and n_2 of the medium on both sides. For a beam in the medium of index n_1, $r = \frac{n_1-n_2}{n_1+n_2}$. The reflection coefficient is thus positive when the beam is reflected inside the mirror and negative when it is reflected inside vacuum.

at pulsation Ω (6.26 MHz for Virgo) with a modulation depth m. The field entering the interferometer is then:

$$E(t) = Ae^{j\omega_0 t}e^{jm\sin(\Omega t)} \tag{15}$$

The term $e^{jm\sin(\Omega t)}$ can be developped using the Bessel functions:

$$e^{jm\sin(\Omega t)} = J_0(m) + J_1(m)e^{j\Omega t} - J_1(m)e^{-j\Omega t} + \text{higher order terms} \tag{16}$$

The entering field can then be written:

$$E(t) = AJ_0(m)e^{j\omega_0 t} + AJ_1(m)e^{j(\omega_0+\Omega)t} - AJ_1(m)e^{j(\omega_0-\Omega)t} \tag{17}$$

It is the superposition of a wave with pulsation ω_0 called the carrier and two waves of pulsations $\omega_0 \pm \Omega$ called the sidebands. The amplitude of the waves depends on the modulation depth m.

The field transmitted by the interferometer can be written (applying equation 11 to the carrier and lateral bands):

$$E^t(t) = A_0^t J_0 e^{j\omega_0 t} + A_+^t J_1 e^{j(\omega_0+\Omega)t} - A_-^t J_1 e^{j(\omega_0-\Omega)t} \tag{18}$$

$$(A_0^t J_0) = AJ_0 e^{jk_0 l_+}\left[jr\sin(k_0 l_-) + \Delta r\cos(k_0 l_-)\right] \tag{19}$$

$$(A_+^t J_1) = AJ_1 e^{jk_+ l_+}\left[jr_{sb}\sin k_+ l_- + \Delta r_{sb}\cos(k_+ l_-)\right] \tag{20}$$

$$(-A_-^t J_1) = -AJ_1 e^{jk_- l_+}\left[jr_{sb}\sin k_- l_- + \Delta r_{sb}\cos(k_- l_-)\right] \tag{21}$$

where we defined:

$$k_0 = \frac{\omega_0}{c}, \quad k_+ = \frac{\omega_0+\Omega}{c}, \quad k_- = \frac{\omega_0-\Omega}{c} \tag{22}$$

and where r_{sb} and Δr_{sb} are the average reflectivity and asymmetry of both arms for the side bands[7]

Let's now compute the transmitted power $P^t(t)$:

$$P^t(t) = E^t(t)\overline{E^t(t)} \tag{23}$$

$$\begin{aligned}
= \quad & (A_0^t J_0)(\overline{A_0^t J_0}) + (A_+^t J_1)(\overline{A_+^t J_1}) + (-A_-^t J_1)(\overline{-A_-^t J_1}) \\
+ \quad & (A_0^t J_0)e^{j\omega_0 t}\overline{(A_+^t J_1)}e^{-j(\omega_0+\Omega)t} + (A_0^t J_0)e^{j\omega_0 t}\overline{(-A_-^t J_1)}e^{-j(\omega_0-\Omega)t} \\
+ \quad & (A_+^t J_1)e^{j(\omega_0+\Omega)t}\overline{(A_0^t J_0)}e^{-j\omega_0 t} + (A_+^t J_1)e^{j(\omega_0+\Omega)t}\overline{(-A_-^t J_1)}e^{-j(\omega_0-\Omega)t} \\
+ \quad & (-A_-^t J_1)e^{j(\omega_0-\Omega)t}\overline{(A_0^T J_0)}e^{-j\omega_0 t} + (-A_-^t J_1)e^{j(\omega_0-\Omega)t}\overline{(A_+^t J_1)}e^{-j(\omega_0+\Omega)t}
\end{aligned}$$

$$\begin{aligned}
= \quad & (A_0^t J_0)(\overline{A_0^t J_0}) + (A_+^t J_1)(\overline{A_+^t J_1}) + (A_-^t J_1)(\overline{A_-^t J_1}) \\
+ \quad & \Re\left\{\left[(A_0^t J_0)(\overline{-A_-^t J_1}) + (\overline{A_0^t J_0})(A_+^t J_1)\right]e^{j\Omega t}\right\} \\
+ \quad & \Re\left\{(A_+^t J_1)(\overline{-A_-^t J_1})e^{j2\Omega t}\right\}
\end{aligned} \tag{24}$$

The power transmitted by the interferometer is the sum of a continuous term, a term at the modulation frequency and a term at twice the modulation frequency.

[7] This is the more general case: for a simple interferometer, the reflectivity for the side bands is the same as the one for the carrier.

B.2.1 Continous term of the transmitted power

The continuous term of the transmitted power is the sum of three terms like in the equation 12.

$$\begin{aligned}
P^t_{DC} = & \quad (A^t_0 J_0)(\overline{A^t_0 J_0}) + (A^t_+ J_1)(\overline{A^t_+ J_1}) + (A^t_- J_1)(\overline{A^t_- J_1}) \\
= & \quad \frac{P_0 J_0^2}{2}(r^2+\Delta r^2)\big[1 - C\cos(2k_0 l_-)\big] \\
& + \quad \frac{P_0 J_1^2}{2}(r_{sb}^2+\Delta r_{sb}^2)\big[1 - C_{sb}\cos(2k_+ l_-)\big] \\
& + \quad \frac{P_0 J_1^2}{2}(r_{sb}^2+\Delta r_{sb}^2)\big[1 - C_{sb}\cos(2k_- l_-)\big] \\
= & \quad \frac{P_0 J_0^2}{2}(r^2+\Delta r^2)\big[1 - C\cos(2k_0 l_-)\big] \\
& + \quad \frac{P_0 J_1^2}{2}(r_{sb}^2+\Delta r_{sb}^2)\big[2 - C_{sb}\big(\cos(2k_+ l_-)\cos(2k_- l_-)\big)\big] \\
= & \quad \frac{P_0 J_0^2}{2}(r^2+\Delta r^2)\big[1 - C\cos(2k_0 l_-)\big] \\
& + \quad P_0 J_1^2(r_{sb}^2+\Delta r_{sb}^2)\big[1 - C_{sb}\cos((k_+ + k_-)l_-)\cos((k_+ - k_-)l_-)\big] \\
= & \quad \frac{P_0 J_0^2}{2}(r^2+\Delta r^2)\big[1 - C\cos(2k_0 l_-)\big] \\
& + \quad P_0 J_1^2(r_{sb}^2+\Delta r_{sb}^2)\big[1 - C_{sb}\cos(2k_0 l_-)\cos(\frac{2\Omega l_-}{\mathrm{c}})\big]
\end{aligned} \tag{25}$$

Now assume the usual case where $r_{sb} = r$ and $\Delta r_{sb} = \Delta r$. The phase offset of the Michelson interferometer arms is defined as $\Delta\Phi = 2k_0 l_-$.

$$\begin{aligned}
P^t_{DC} &= P_0(r^2+\Delta r^2)\left[\frac{J_0^2}{2}\big(1 - C\cos(\Delta\Phi)\big) + J_1^2\big(1 - C\cos(\frac{2\Omega l_-}{\mathrm{c}})\cos(\Delta\Phi)\big)\right] \\
&= P_0(r^2+\Delta r^2)\left[\big(\frac{J_0^2}{2} + J_1^2\big) - \big(\frac{J_0^2}{2} + J_1^2\cos(\frac{2\Omega l_-}{\mathrm{c}})\big)C\cos(\Delta\Phi)\right] \\
&= \beta\big(1 - \gamma\cos(\Delta\Phi)\big)
\end{aligned} \tag{26}$$

where we defined, using the sideband transmission factor $T = \sin^2(\frac{\Omega l_-}{\mathrm{c}})$:

$$\beta = P_0\left(\frac{J_0^2}{2} + J_1^2\right)\big(r^2+\Delta r^2\big) \tag{27}$$

$$\gamma = \left[1 - \frac{2J_1^2}{\frac{J_0^2}{2} + J_1^2}T\right]C \tag{28}$$

β is proportional to the laser power, and depends on the reflection coefficients and modulation depth. γ is proportional to the interferometer contrast and also depends on the modulation

depth. The sideband transmission factor T is a function of l_- which varies of a few μm when data are taken in free swinging Michelson configuration. However, the period of the factor is of the order of 50 m. Its variations over a few microns can thus be neglected.

In the case of no modulation ($J_0 = 1$ and $J_1 = 0$), the equation is the same as equation 12. If the sidebands are not transmitted ($T = 0$), the γ factor corresponds to the interferometer contrast.

Some numerical values The expected values of β/P_0 and of γ can be estimated for different IFO configurations, using the mirror and length characteristics from appendix A (with $m = 0.27$). It is assumed that the transmission and reflection coefficients of the mis-aligned mirrors (by a few 100 μrad are the same as when the mirrors are aligned.

The Bessel coefficients for a modulation depth $m = 0.27$ are $J_0 = 0.9818$ and $J_1 = 0.1338$.

	NE-WI	WE-NI	NI-WI
T	0.01568	0.0261	0.0003
γ/C	0.9989	0.9981	1.000
C	0.247	0.245	1.0
γ	0.247	0.244	1.0
β/P_0	0.224	0.224	0.441

Table 5: Some numerical values of the coefficients that enter the P^t_{DC} expression (equation 26). They all are of dimensin [1]. P_0 is the power impinging on the BS at the IFO entrance.

B.2.2 Term of the transmitted power at the modulation frequency

The term of pulsation Ω of the transmitted power is computed from equation 24.

$$P^t_\Omega(t) = \Re\left\{\left[(A^t_0 J_0)(\overline{-A^t_- J_1}) + (\overline{A^t_0 J_0})(A^t_+ J_1)\right] e^{j\Omega t}\right\} \tag{29}$$

$$= A\bar{A}J_0J_1\Re\Big\{ -e^{jk_0l_+}\big(jr\sin(k_0l_-) + \Delta r\cos(k_0l_-)\big)e^{-jk_-l_+}\big(-jr_{sb}\sin(k_-l_-) + \Delta r_{sb}\cos(k_-l_-)\big)e^{j\Omega t}$$
$$+e^{-jk_0l_+}\big(-jr\sin(k_0l_-) + \Delta r\cos(k_0l_-)\big)e^{jk_+l_+}\big(jr_{sb}\sin(k_+l_-) + \Delta r_{sb}\cos(k_+l_-)\big)e^{j\Omega t}\Big\}$$

$$P^t_\Omega(t) = P_0 J_0 J_1 \Re\Big\{ e^{j\left(\frac{\Omega}{c} l_+ + \Omega t\right)} \big[\quad -jr\sin(k_0 l_-) \quad jr_{sb}\big(\sin(k_+ l_-) - \sin(k_- l_-)\big) \quad (30)$$

$$-jr\sin(k_0 l_-) \quad \Delta r_{sb}\big(\cos(k_+ l_-) + \cos(k_- l_-)\big)$$

$$+\Delta r\cos(k_0 l_-) \quad jr_{sb}\big(\sin(k_+ l_-) + \sin(k_- l_-)\big)$$

$$+\Delta r\cos(k_0 l_-) \quad j\Delta r_{sb}\big(\cos(k_+ l_-) - \cos(k_- l_-)\big) \quad \big] \Big\}$$

$$= P_0 J_0 J_1 \Re\Big\{ e^{j\left(\frac{\Omega}{c} l_+ + \Omega t\right)} \big[\quad 2rr_{sb}\sin(k_0 l_-)\cos\big(\frac{\omega_0}{c} l_-\big)\sin\big(\frac{\Omega}{c} l_-\big) \quad (31)$$

$$-2\Delta r\Delta r_{sb}\cos(k_0 l_-)\sin\big(\frac{\omega_0}{c} l_-\big)\sin\big(\frac{\Omega}{c} l_-\big)$$

$$-2jr\Delta r_{sb}\sin(k_0 l_-)\cos\big(\frac{\omega_0}{c} l_-\big)\cos\big(\frac{\Omega}{c} l_-\big)$$

$$+2jr_{sb}\Delta r\cos(k_0 l_-)\sin\big(\frac{\omega_0}{c} l_-\big)\cos\big(\frac{\Omega}{c} l_-\big) \quad \big] \Big\}$$

$$P^t_\Omega(t) = 2P_0 J_0 J_1 \Re\Big\{ \quad e^{j\frac{\Omega}{c} l_+ + \Omega t}\frac{1}{2}\sin(2k_0 l_-)\Big[\sin\big(\frac{\Omega}{c} l_-\big)[rr_{sb} - \Delta r\Delta r_{sb}] \quad (32)$$

$$+ j\cos\big(\frac{\Omega}{c} l_-\big)[r_{sb}\Delta r - r\Delta r_{sb}] \quad \Big] \Big\}$$

$$P^t_\Omega(t) = P_0 J_0 J_1 \sin(\Delta\Phi)\Big[\quad \cos(\frac{\Omega}{c} l_+ + \Omega t)\sin(\frac{\Omega}{c} l_-) \quad (rr_{sb} - \Delta r\Delta r_{sb}) \quad (33)$$

$$-\sin(\frac{\Omega}{c} l_+ + \Omega t)\cos(\frac{\Omega}{c} l_-) \quad (r_{sb}\Delta r - r\Delta r_{sb})\Big]$$

Demodulated signals - The transmitted power measured by the B1p photodiodes is demodulated at the modulation frequency Ω. The phase φ of the demodulation is adjusted for Science Mode data and not to the phase $\Psi = \frac{\Omega}{c} l_+$ of the free swinging Michelson data.

The demodulated signal 'in phase', P_{ACp}, is computed multiplying the power $P^t_\Omega(t)$ by $\cos(\Omega t + \varphi)$ and low-pass filtering the result in order to keep the continuous component only. One has:

$$\begin{aligned} \cos(\Psi + \Omega t)\cos(\Omega t + \varphi) &= \tfrac{1}{2}\Big[\cos(\Psi + \varphi + 2\Omega t) + \cos(\Psi - \varphi)\Big] \\ \sin(\Psi + \Omega t)\cos(\Omega t + \varphi) &= \tfrac{1}{2}\Big[\sin(\Psi + \varphi + 2\Omega t) + \sin(\Psi - \varphi)\Big] \end{aligned}$$

Reporting these formulas in equation (33) and keeping only the continuous term (and not the term at 2Ω), one gets the demodulated signal in phase:

$$\begin{aligned} P_{ACp} = \; & \tfrac{1}{2} P_0 J_0 J_1 \sin(\Delta\Phi) \Big[\quad \sin\left(\tfrac{\Omega}{c} l_-\right)(r r_{sb} - \Delta r \Delta r_{sb}) \cos(\Psi - \varphi) \\ & \qquad\qquad - \cos\left(\tfrac{\Omega}{c} l_-\right)(r_{sb}\Delta r - r \Delta r_{sb}) \sin(\Psi - \varphi) \quad \Big] \\ = \; & \alpha_{ACp} \sin(\Delta\Phi) \end{aligned}$$

Similarly, the demodulated signal 'in quadrature', P_{ACq}, is computed multiplying the power $P^t_\Omega(t)$ by $\sin(\Omega t + \varphi)$ and low-pass filtering the result in order to keep the continuous component only. One founds:

$$\begin{aligned} P_{ACq} = \; & -\tfrac{1}{2} P_0 J_0 J_1 \sin(\Delta\Phi) \Big[\quad \sin\left(\tfrac{\Omega}{c} l_-\right)(r r_{sb} - \Delta r \Delta r_{sb}) \sin(\Psi - \varphi) \\ & \qquad\qquad + \cos\left(\tfrac{\Omega}{c} l_-\right)(r_{sb}\Delta r - r \Delta r_{sb}) \cos(\Psi - \varphi) \quad \Big] \\ = \; & \alpha_{ACq} \sin(\Delta\Phi) \end{aligned}$$

In general, the reflection coefficients are the same for the carrier and the sidebands. The second term, with the difference $r_{sb}\Delta r - r\Delta r_{sb}$ is thus negligible. Moreover, $r^2 \sim 0.8$, $r\Delta r \sim 0.1$ and $\Delta r^2 \sim 0.01$. Neglecting the terms containing Δr, the demodulated powers can be written:

$$P_{ACp} \sim \alpha' \cos(\Psi - \varphi) \sin(\Delta\Phi) \tag{34}$$

$$P_{ACq} \sim -\alpha' \sin(\Psi - \varphi) \sin(\Delta\Phi) \tag{35}$$

$$\alpha' = \frac{1}{2} P_0 J_0 J_1 \sin\left(\frac{\Omega}{c} l_-\right) r^2 \tag{36}$$

Both of them can be written as

$$P_{AC} = \alpha_{AC} \sin(\Delta\Phi) \tag{37}$$

The factors α_{AC} are different for both demodulated signals. They are proportional to the laser power. They depend on the modulation depth and on the mirror reflectivities. They also depend on the sideband transmission and reflection factors T and $1 - T$, i.e. on l_- (thus on $\Delta\Phi$). There period, of the order of 50 m, is much larger than the mirror motion, of the order of microns in the free swinging Michelson data. Their variations can thus be neglected. For a given Michelson configuration, the difference between the ACp and ACq signals is the cosine or sine factor of the phase shift between Ψ and the phase φ of the demodulation. In principle, one could set the phase of the demodulation such that one signal achieve optimum sensitivity while the other is zero.

B.3 Conclusion

The continuous and demodulated signal at the output of a frontal phase modulated Michelson interferometer are functions of the phase offset between the two arms $\Delta\Phi$:

$$P_{DC} = \beta\big(1 - \gamma\cos(\Delta\Phi)\big) \quad (38)$$

$$P_{ACp} = \alpha_{ACp}\sin(\Delta\Phi) \quad (39)$$

$$P_{ACq} = \alpha_{ACq}\sin(\Delta\Phi) \quad (40)$$

where β, α_{ACp} and α_{ACq} are proportional to the laser power, and γ is proportional to the interferometer contrast.

A demodulated signal can be combined with the continuous signal to reconstruct the phase offset vs time, and thus the differential arm length variations $\Delta L(t) = \frac{\lambda}{4\pi}\Delta\Phi(t)$. This is the base of the calibration of the Virgo mirror actuation transfer functions.

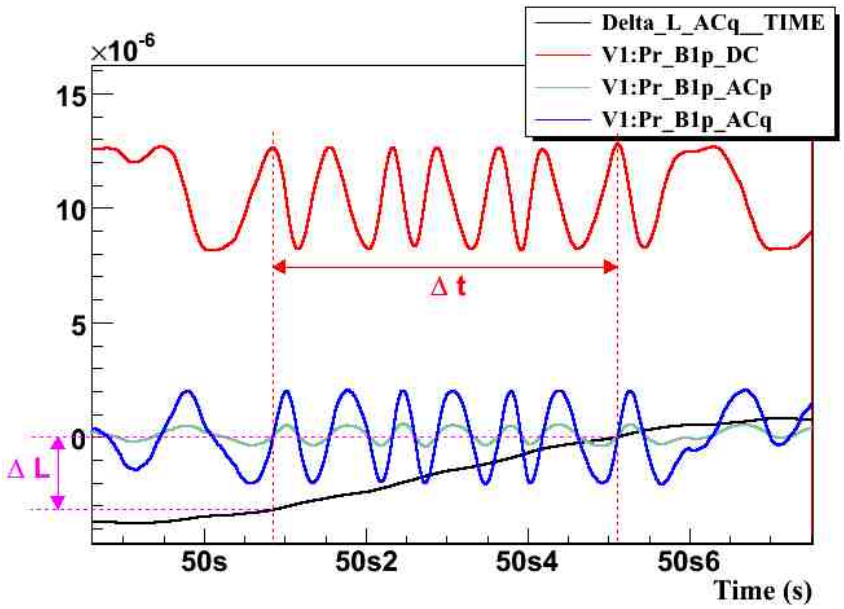

Figure 13: DC, ACp and ACq powers (along with the reconstructed ΔL channel) in WE-NI asymmetric data. The ACp and ACq powers are in phase as expected from equation 34 (or phase opposition). The DC power is always strictly positive since the contrast in not 1 in asymmetric configurations. On the bright fringe (DC is maximum) and on the dark fringes (DC is minimum), the AC signals cross zero as expected. The y-axis scale units depends on the signals: 20 W for DC power, 10 W for ACp and ACq powers (1 m for ΔL). Dark fringe counting, as in section 2.3.3: during the time Δt, the DC signal shows that the differential mirror motion has crossed 6 interfringes, thus $6 \times \lambda/2 = 3.19\,\mu$m. During the same time, the reconstructed channel shows a mirror motion of $\Delta L \sim 3.18\,\mu$m.

C MinMax method algorithm

The details of the algorithms are given here.

The parameters α, β and γ are estimated from the minimum, maximum and average signals each time the angle $\Delta\Phi$ has moved by more than 2π since last estimation (or if more than 5 s of data was read for the very first computation).

They are then averaged using a sliding average that behaves as a low pass filter.

The value of $\Delta\Phi_i$ and ΔL_i are then estimated for every sample i from the last average values $<\alpha>_k$, $<\beta>_k$ and $<\gamma>_k$. The ΔL_i values are saved into the frame at the same rate as the sampling of the photodiode signals Pr_B1p.

Two values of ΔL are computed, one using Pr_B1p_ACq and the other one using Pr_B1p_ACp.

The parameter average values $<\alpha>_k$, $<\beta>_k$ and $<\gamma>_k$ are saved into the frame at the same rate as the photodiode signal with names $MinMax\_A\_ACq$, $MinMax\_B\_ACq$, $MinMax\_C\_ACq$ respectively (if they are computed with the quadrature signal ACq).

D Ellipse method algorithm

The *Ellipse* method is used to estimate the mirror displacement in free Michelson configuration. The details of the algorithm are given here. It is based on the fact that the phase (Pr_B1p_ACp) or quadrature (Pr_B1p_ACq) photodiode signals plotted as function of the DC signal has an elliptic shape.

D.1 General algorithm

Two values of ΔL are estimated from both the phase and quadrature signals. The following examples are given for the quadrature signal.

The kth averaged ellipse centre position (X_0^k, Y_0^k) and axis width ratio σ_X^k/σ_Y^k are estimated from the DC and ACq signals. Then the angle $\Delta\Phi_i$ of the following samples i are estimated from the relation:

$$\cos\Delta\Phi_i = \frac{DC_i - X_0^k}{\sigma_X^k} \tag{41}$$

$$\sin\Delta\Phi_i = \frac{ACq_i - Y_0^k}{\sigma_Y^k} \tag{42}$$

$$\tag{43}$$

The current ellipse parameters x_0^k, y_0^k, σ_x^k, σ_y^k are estimated using the method described below from buffered samples of DC and ACq signals every time that the current $\Delta\Phi_k$ differs by more than 2π from its value when the last ellipse $\Delta\Phi_{k-1}$ was fitted and that the number of samples in the buffer is more than 1000 (the first ellipse is computed using 5 s of data). They are then average using a sliding average.

The estimated values of ΔL as well as the estimated values of the averaged ellipse parameters are saved into the frame at the same rate as the photodiode signals.

D.2 Ellipse fitting method algorithm

A numerically stable non-iterative algorithm for fitting an ellipse to a set of data points is described in [5]. It has been added in the *Cali* module using the matrix objects from ROOT in the files *FreeMichelsonCalib_DeltaLReconstruction*, under the name *HalirFlusserMethod*.

Ellipse fitting method description - The method takes as arguments a set of N coordinates (x_i, y_i), $i \subset (1, N)$. The ellipse is described by an implicit second order polynomial:

$$F(x, y) = ax^2 + bxy + cy2 + dx + ey + f = 0$$

and the six unknown ellipse parameters are (a, b, c, d, e, f).

From the data, two $N \times 3$ matrixes are built:

$$D_1 = \begin{pmatrix} x_1^2 & x_1 y_1 & y_1^2 \\ . & . & . \\ . & . & . \\ x_i^2 & x_i y_i & y_i^2 \\ . & . & . \\ . & . & . \\ x_N^2 & x_N y_N & y_N^2 \end{pmatrix}$$

$$D_2 = \begin{pmatrix} x_1 & y_1 & 1 \\ . & . & . \\ . & . & . \\ x_i & y_i & 1 \\ . & . & . \\ . & . & . \\ x_N & y_N & 1 \end{pmatrix}$$

Then, four 3×3 matrixes are defined:

$$S_1 = D_1^T \times D_1 \quad (44)$$
$$S_2 = D_1^T \times D_2 \quad (45)$$
$$S_3 = D_2^T \times D_2 \quad (46)$$
$$(47)$$

and

$$C_1 = \begin{pmatrix} 0 & 0 & 1/2 \\ 0 & -1 & 0 \\ 1/2 & 0 & 0 \end{pmatrix}$$

From these objects, one computes the 3×3 matrix M:

$$M = C_1^{-1} \left(S_1 - S_2 S_3^{-1} S_2^T \right)$$

The three eigenvectors v_j of M are then calculated. One of these vectors, called $a_1 = (a, b, c)$, represents the ellipse parameters. To choose among them, one estimates the number $s = a_1^T C_1 a_1$ and select the vector a_1 with the more little positive s value. The other ellipse parameters are then calculated as:

$$a_2 = -S_3^{-1} S_2^T a_1 = (d, e, f)$$

At this point, the six parameters (a, b, c, d, e, f) are fitted.

As the fitted ellipse of the AC vs DC signals has its main axis parallel to x and y:

$$\frac{(x - x_0)^2}{\sigma_x^2} + \frac{(y - y_0)^2}{\sigma_y^2} = 1$$

one can deduce from the parameters the ellipse center coordinates (x_0, y_0) and the normalized axis lengths (σ_x, σ_y):

$$\sigma_x^2 = \frac{1}{a} \tag{48}$$

$$\sigma_y^2 = \frac{1}{c} \tag{49}$$

$$x_0 = -\frac{\sigma_x^2 \times d}{2} \tag{50}$$

$$y_0 = -\frac{\sigma_y^2 \times e}{2} \tag{51}$$

These four parameters are returned by the HalirFlusserMethod function and used to average the ellipse parameters over time and to compute the $\Delta\Phi$ angle of the following data points.

The resolution of the ellipse centre and sigma reconstruction has been estimated and is better than 1%.

E Sliding average

A low-pass filter is used to smooth the parameters computed for the ΔL estimation in free Michelson configuration. The method is a sliding average that uses all the data in the past. One needs to define a parameter ϵ. The raw data being called $(a_k)_{k=0..N}$, the average of a at the step i is defined as:

$$\overline{a_0} = a_0 \tag{52}$$

$$\overline{a_i} = \epsilon \times \overline{a_{i-1}} + (1 - \epsilon) \times a_i \tag{53}$$

$$\overline{a_i} = \epsilon^i \times a_0 + (1 - \epsilon) \sum_{k=1}^{i} \epsilon^{i-k} a_k \tag{54}$$

Assuming that ϵ is 0.9, the last term contributes for 10% to the average. The further the data is, the lower it contributes (through the factor $(1 - \epsilon) \times \epsilon^{i-k}$).

F SIESTA configuration file

Configuration file for SIESTA simulation of an asymmetric WE-NI Michelson interferometer, with white noise injection on the WE mirror.

```
/* Simulate 10 s of data at 1 MHz (for delay studies) */
UJclock masterClocks 10000000 2 1000000 1.   /*clock rate for OPseq : 100 kHz to 40 MHz */
UFrBuilder FBuilder 1 0 0 1

/* Seismic noise */
/* Noise motion description */
GRound 0  3.e-9 0.1  0.
/* Noise motion at on point */
GRoundPt Mbs  0.     0.     0.
GRoundPt Mni  6.2    0.     0.
GRoundPt Mne  3006.2 0.     0.
GRoundPt Mwi  0.     5.8    0.
GRoundPt Mwe  0.     3005.8 0.
GRoundPt Mpr -6.0    0.     0.

/*  ------------------------------------------------- */
/* Generate white noise for injection to the mirrors */
/* USgenerator [name][clock][sigma] */
USgenerator    wn_0     0    0.00004

/* Force applied on the mirrors */
/* BS: no noise */
USadder fBS 0 1 wn_0.out
                0.0
/* WE: noise */
USadder fWE 0 1 wn_0.out
                100.0
/* NI: no noise */
USadder fNI 0 1 wn_0.out
                0.0

/* Mechanical simulation, with thermal noise */

/* BS front */
MIglobal    mBS  0  Mbs.dxyzt  NULL  NULL  NULL fBS.out  10
100. 100. 100. 100. 100. 100. 100. 60.  28. 28.
1.   1.   1.   1.   1.   1.   1.   1.   .7   .7
```

```
1.e2 1.e2 1.e2 1.e2 1.e2 1.e2 1.e2 1.e2 1.e6 1.e6
Thermal  ThBS 0 1 28. 0.5955 1.e6
MIrror   MirBS 0 mBS.dxyzt ThBS.out MiSuBSf NULL 0. 0. 0. .7 -.7 0.
MIsurf   MiSuBSf  0.  .2  0.  0.  0.  .5  0.

/*NI back */
MIglobal    mNI  0  Mni.dxyzt  NULL  NULL  NULL  fNI.out  10
100. 100. 100. 100. 100. 100. 100. 60.  28. 28.
1.   1.   1.   1.   1.   1.   1.   1.   .7   .7
1.e2 1.e2 1.e2 1.e2 1.e2 1.e2 1.e2 1.e2 1.e6 1.e6
Thermal  ThNI 0 1 28. 0.5955 1.e6
MIrror   MirNI 0 mNI.dxyzt ThNI.out NULL MiSuNIb 6.2 0. 0. 1. 0. 0.
MIsurf   MiSuNIb  0.  .2  0.  0.  0.  .88  3.e-4

/*WE front */
MIglobal    mWE  0  Mwe.dxyzt  NULL  NULL  NULL fWE.out  10
100. 100. 100. 100. 100. 100. 100. 60. 28. 28.
1.   1.   1.   1.   1.   1.   1.   1.   .7   .7
1.e2 1.e2 1.e2 1.e2 1.e2 1.e2 1.e2 1.e2 1.e6 1.e6
Thermal  ThWE 0 1 28. 0.5955 1.e6
MIrror   MirWE 0 mWE.dxyzt ThWE.out MiSuWEf NULL 0. 3005.8 0. 0. 1. 0.
MIsurf   MiSuWEf  2.898e-4  .2  0.  0.  0.  .9999  0.


/* Misaligned mirrors: null reflection coefficients */
/*NE front */
MIrror   MirNE 0 NULL NULL MiSuNEf NULL 3006.2 0. 0. 1. 0. 0.
MIsurf   MiSuNEf 0. .2  0. 0. 0. 0. 0.
/*WI back */
MIrror   MirWI 0 NULL NULL NULL MiSuWIb  0. 5.8 0. 0. 1. 0.
MIsurf   MiSuWIb 0. .2  0. 0. 0. 0. 0.
/* PR front */
MIrror   MirPR 0 NULL NULL MiSuPRf NULL -6. 0. 0. 1. 0. 0.
MIsurf   MiSuPRf 0. .2  0. 0. 0. 0. 0.

/* Optics simulation */
IOlaser laser 0 NULL 1.064e-6 10. NULL NULL -8.8879408e-6  .0198008 .40 NO 0
OPmod   mod   0 laser.oBeam 3 0. 6.268428e6 -6.268428e6 carrier NULL sb1 NULL sb2 NULL
USignal carrier  0.96
USignal sb1 0.196
USignal sb2 -0.196
```

```
/* Simulation of the full interferometer */
OPseq  itf 0 mod.oBeam MiSuBSf MiSuNIb MiSuNEf MiSuWIb MiSuWEf MiSuPRf YES YES

/* Detection photodiode, with shot noise */
OPdiode d1 0 1. 6.268428e6 NULL itf.oBeam1 YES

/* Output channels */
/* -> Demodulated detection photodiode signals */
UFrLRdout 0 "Pr_B1p_DC"    d1.dc    1.0 -1 adc
UFrLRdout 0 "Pr_B1p_ACp"   d1.phase 1.0 -1 adc
UFrLRdout 0 "Pr_B1p_ACq"   d1.quad  1.0 -1 adc
/* -> Force applied to the mirror */
UFrLRdout 0 "Sc_BS_zCorr"   fBS.out  1.0 -1 adc
UFrLRdout 0 "Sc_WE_zCorr"   fWE.out  1.0 -1 adc
UFrLRdout 0 "Sc_NI_zCorr"   fNI.out  1.0 -1 adc
/* -> Mirror motion */
UFrLRdout 0 "MirBS"  MirBS.dxyzt.s2     1.0 -1 adc
UFrLRdout 0 "MirWE"  MirWE.dxyzt.s2     1.0 -1 adc
UFrLRdout 0 "MirNI"  MirNI.dxyzt.s2     1.0 -1 adc

UFrOFile -1 "FreeMichelsonSimulation_WENI"   NO FBuilder.frameH 10
```

References

[1] Fabrice Beauville, PhD manuscript, 2005 (LAPP-T-2005-07)

[2] Olivier Véziant, PhD manuscript, 2003

[3] R. Flaminio, F. Marion, B. Mours, O. Véziant, Virgo note (2002) VIR-NOT-LAP-1390-204

[4] L. Rolland F. Marion, B. Mours, Virgo note (2008) VIR-015-08B

[5] R. Halir and J. Flusser, *Numerically stable direct least squares fitting of ellipses*, in Skala, V(ed.)Proc.Int.Conf. in Central Europe on Computer Graphics, Vizualisation and Interactive Digital Media, 125–132 (1998)

[6] B. Caron et al. **Astroparticle Physics 10**, 369-386 (1999) *SIESTA, a time domain, general purpose simulation program for the VIRGO experiment*